Spectral modeling of laser systems with diffractive cavities

Journal of Physics: Photonics

OPEN ACCESS

RECEIVED
16 December 2025

REVISED
10 April 2026

ACCEPTED FOR PUBLICATION
24 April 2026

PUBLISHED
11 May 2026

PAPER

Spectral modeling of laser systems with diffractive cavities

Hendrik Büker[1,2,*], **Marc Eichhorn**[2,3], **Katerina Chrysalidis**[1] and **Eduardo Granados**[1]

[1] European Organization for Nuclear Research (CERN), Espl. des Particules 1, 1217 Genéve, Switzerland
[2] Karlsruhe Institute of Technology (KIT), Institute of Control Systems (IRS), Fritz-Haber-Weg 1, 76131 Karlsruhe, Germany
[3] Fraunhofer IOSB (Institute of Optronics, System Technologies and Image Exploitation), Gutleuthausstr. 1, 76275 Ettlingen, Germany
[*] Author to whom any correspondence should be addressed.

E-mail: hendrik.buker@cern.ch

Keywords: spectral modeling, ray-matrices, narrow-linewidth, tunable lasers, gain-switched lasers

Supplementary material for this article is available online

Abstract

We present a comprehensive modeling framework for predicting the spectral output of pulsed, narrow-linewidth lasers based on dispersive optical resonators. Our approach integrates polarization-dependent losses, mode steering, and dispersive effects within a unified round-trip matrix formalism, enabling the calculation of a wavelength-dependent resonator feedback function. By combining this feedback function with transient gain dynamics, the model provides estimates of the energy distribution among longitudinal modes and resulting laser linewidths for lasers in transient regime. The linewidths predictable by our model spans from a few hundreds MHz, limited by spectral phase noise, and up to tens of GHz, limited by temporal resolution of the gain dynamics simulation. We compare the simulation results with experimental measurements of Ti:Sapphire laser configurations with intra-cavity etalons, birefringent filters, and diffraction gratings. The agreement with experimental results demonstrates that this framework offers a practical tool for resonator design and optimization, bridging the gap between traditional element-wise analysis and holistic spectral prediction. Our method supports the development of tunable, narrow-linewidth lasers for applications such as resonance-ionization and high-resolution spectroscopy.

1. Introduction

Widely tunable and narrow-linewidth lasers are of paramount importance for the precise control and measurement of light–matter interactions, particularly with atoms and molecules [1]. Fine- or hyperfine-splitting arising from magnetic moments or spin–orbit coupling in atoms can be studied by spectrally resolving the transition-of-interest linewidth, typically in the order of several tens of MHz to a few GHz [2, 3]. Geometric arrangements to reduce the Doppler broadening are required for precise measurement, as well as laser linewidth comparable to, or lower than, the transition linewidth itself. Here, single longitudinal mode lasers with linewidth ranging from a few Hz to several hundred MHz are necessary [4–6].

Narrow-linewidth lasers can also be employed to selectively ionize isotopes in a gas mixture through sequential resonant excitation, this method is known as resonance-ionization spectroscopy (RIS). For this purpose, the lasers must not only be precisely wavelength tuned to the relevant transitions but also their linewidth must match each Doppler broadened transition width to increase ionization efficiency [7]. This broadening can be up to several tens of GHz for ions produced in hot cavity environments [8, 9].

In RIS, efficient ionization typically requires ns-pulsed lasers with kW peak power to saturate the atomic transitions. For this purpose, Gain- or Q-switched lasers are utilized as they readily fulfill these peak power requirements exploiting high single-pass optical gain and can provide a suitable spectral width. Most importantly, wavelength coverage is a fundamental aspect to be taken into account, as

some of the transitions-of-interest are in hard to reach spectral regions, like the visible or deep ultraviolet (DUV) region, where there are very few suitable solid-state gain media [10]. To extend the spectral coverage, non-linear effects can be employed, such as second $\chi^{(2)}$ or third order $\chi^{(3)}$ nonlinear effects, including harmonic generation, frequency mixing [11] or stimulated Raman scattering [9] among others.

To achieve broad spectral coverage, dispersive and spectrally selective elements are routinely employed in gain-switched laser oscillators [12]. Here, the accumulated round-trip spatio-temporal dispersion and diffraction govern the output central wavelength and spectral linewidth by imposing mode-dependent losses that limit the number of longitudinal modes able to oscillate simultaneously. As the pulse formation in ns-pulsed lasers occurs inherently in a transient regime, an accurate and direct prediction of the number of modes, and hence the output linewidth, can be challenging.

To date, numerous models and formalisms have been developed to describe the interaction between light and the dispersive components. However, these approaches generally treat the individual effects of isolated elements within the laser cavity. This paper proposes a holistic methodology to calculate the laser spectral output by employing analytical and numerical methods describing the laser gain–loss dynamics that govern the spectral characteristic in the transient regime.

2. Theoretical model

The output spectrum of a multi-axial-mode pulse is governed by the number of oscillating longitudinal modes and their energy distribution. In the absence of spatial or spectral hole burning, direct gain–loss dynamics dictate the output multi-mode spectrum energy distribution. Adopting these approximations, we propose a general model that includes different coupling and loss mechanisms that conform the spectral resonator feedback function $\Theta(\lambda)$. Together with the resonator time-dependent gain function $\Gamma(t,\lambda)$, we are ready to calculate the energy spectrum and resulting linewidth.

The resonator feedback function depends on the choice of laser cavity elements. Since the early 70 s, matrix formalisms have been used to characterize the response of optical elements and resonators [13, 14]. The addition of dispersive optical elements in cavities was first described by F. J. Duarte and J. Piper in the early 80 s, when they proposed mathematical methods to calculate multi-prism optical system response. The results supported the optimization of narrow-linewidth dye lasers [12, 15–17]. By the late 80 s, O. E. Martinez already introduced a 3×3 matrix formalism to study laser cavities with dispersive elements such as gratings or prisms [18].

Most of the work considering dispersion aims to compensate it for mode-locking and ultrashort pulses. Duarte and Martinez have made efforts to predict the behavior of a laser resonator with a bandwidth limited by diffraction [17, 18]. Duarte uses the resolving power of the diffractive element in the resonator to estimate the resulting laser linewidth. Martinez considers the spatial mode in the resonator and introduces a Gaussian aperture to approximate mode-coupling. All these models are not fully taking into account the mode-coupling after each pass for individual wavelengths or considering polarization effects and gain dynamics.

Shortly after, A. G. Kostenbauder offered an extended formalism including spatio-temporal coupling by introducing additional terms in a 4×4 matrix, widely used for the calculation of dispersion compensation in broad-band oscillators, pulse stretchers and compressors [19]. Following this work, O. E. Martinez and J. L. A. Chilla used a similar method to calculate dispersion management in mode-locked lasers [20]. More recently, these techniques were further developed and found use in increasingly complex systems [21–23].

In these methods, a broad range of systems can be modeled already, however, several effects were neglected. Among them, the coupling between polarization and diffractive effects or the mode resonator coupling factors after a cavity round-trip. Note that the proposed model, described in the following is equivalent to existing ones for resonator configurations where these effects are not dominant, like planar resonator configuration without polarizing elements. Moreover, our model includes temporal domain calculations of gain media, predicting accurately the output spectrum.

2.1. Resonator feedback function

Here, we build on the previous knowledge utilizing a round-trip matrix (RTM) formalism and expand it specifically for pulsed ns narrow-linewidth lasers used in RIS. We will attempt to predict longitudinal multi-mode behavior, and provide an entry point for subsequent time resolved simulation of gain dynamics by modeling $\Theta(\lambda)$. To do this, we propose a specific RTM formalism that includes the general resonator mode design, as well as the description of dispersive effects and polarization. This unified approach further enables us to take into account the interaction between different effects, which was

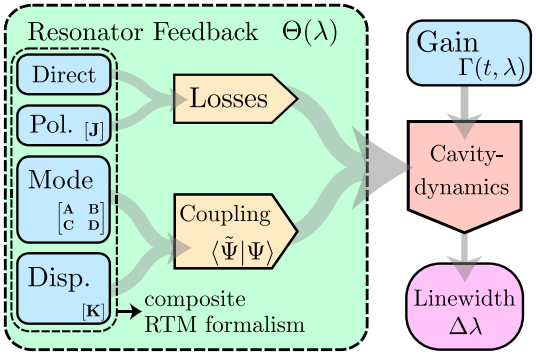

Figure 1. Flow diagram of the modeling approach [24]. Reprinted with permission from [24] © The optical Society. The composite round-trip matrix (RTM) combines the direct and polarization influenced losses with a description of beam-steering effects from dispersive and diffractive effects. The resulting resonator feedback function $\Theta(\lambda)$ and the gain function $\Gamma(t,\lambda)$ are used to calculate the intra-cavity energy dynamics, which allows for calculation of different performance parameters of the laser, like the linewidth $\Delta\lambda$.

usually neglected in previous works. Once $\Theta(\lambda)$ is calculated, gain dynamics (mainly pulse build-up and gain depletion) will ultimately determine the distribution of energy among the axial modes, as depicted in figure 1. The final estimated spectrum can be obtained through a time and spectrally resolved laser rate-equation analysis.

Figure 1 summarizes the various effects co-existing in the laser resonator captured by our model. We focus on two main classes of effects that determine the resonator feedback: (i) direct and polarization-dependent attenuation of a mode, and (ii) mode steering and resulting coupling losses arising from diffractive effects. Direct losses include coating imperfections, interfaces, Fresnel reflections or material absorption, to name a few. Generally these contributions depend on the polarization state $\mathbf{P}$, and their composite effect is included in the transmission function $\alpha_{\mathbf{P}}$. Effects that steer a particular axial mode away from the resonator spatial eigenmode give rise to the effective coupling function η.

For the calculation of $\Theta(\lambda)$, different contributions from each cavity element e_i are taken into account. The resulting axial mode feedback function is the conjunction of described effects and can be written as:

$$\Theta(\lambda) = \alpha_{\mathbf{P}}(\lambda) \times \eta(\lambda) \tag{1}$$

Filtering can be provided by Lyot-filters, acting on the polarization state of the light, and one or several etalons filters which limit the lasing bandwidth. Different models and formalisms have been proposed to describe the effect of these components and their interaction with light separately [12, 19, 25, 26]. Polarization effects can be calculated by using the well-known Jones calculus, in which matrices provide a method to estimate the resulting polarization states of a beam traveling through homogeneous isotropic media and optical devices [25]. In combination with Fresnel reflection formulas, they can be used to calculate the attenuation of polarization-based filters or Brewster-angled interfaces.

2.1.1. Transmission function $\alpha_{\mathbf{P}}(\lambda)$

For calculating the spectral attenuation function we analyze the spectral transmission function of each cavity element e_i, denoted as $\alpha_{\mathbf{P}}(e_i,\lambda)$. We include the polarization dependent reflectivities of mirror and polarizer coatings as losses $\alpha_{\mathbf{P}}(e_i,\lambda) = R(\mathbf{P},\lambda)$. The absorption loss $\Lambda_{\mathbf{P}}(e_i,\lambda) = \int_0^L a(\mathbf{P},\lambda)\mathrm{d}z$ of utilized optical media in cavity elements, can be measured or obtained directly from manufacturers.

The power loss on uncoated elements is calculated by the Fresnel reflection coefficients or manufacturer datasheets. For birefringent filters (BRFs) such as Lyot-filters this can also be addressed by carefully propagating a test beam through all parts of the filter and collecting all individual losses. For etalons and other interference filters the total spectral transmission function $\alpha_{\mathbf{P}}(e_i,\lambda)$ can be calculated from surface reflectivities, material absorption and optical thickness. The spectral functions of these elements can readily give insights to the achievable linewidth of the laser [26].

To obtain the total round-trip transmission function for an axial mode we take the product of the transmission through all optical elements within the resonator.

$$\alpha_{\mathbf{P},\mathrm{tot}}(\lambda) = \prod_i [1 - \Lambda_{\mathbf{P}}(e_i,\lambda)]^{p_i} = \prod_i \alpha_{\mathbf{P}}(e_i,\lambda)^{p_i} \tag{2}$$

Here p_i denotes the number of passes through element e_i during a single round-trip.

2.1.2. Mode coupling

Dispersive and diffractive elements within the laser cavity, depending on the wavelength, may alter the mode direction away from the cavity resonant mode. This steering is equivalent to a loss due to the lack of efficient coupling of the mode after one round trip. As the steering can be evaluated per spectral mode, the feedback contribution cannot be written as function of an individual element, but rather as a function of all the cavity elements together as:

$$\eta(\lambda) = \eta(Q(\lambda), e_1, \cdots, e_n, \mathbf{P}) \tag{3}$$

Where Q is the complex beam parameter for a generalized 2D Gaussian beam spatial representation of an axial resonator mode [27]. To find Q we can utilize an expanded ray-transfer-matrix formalism similar to the ABCD-Matrix [26]. This method is very versatile since while it describes light as a ray, the results can be extrapolated to first order Gaussian modes. To describe the effects of gratings or prisms in a ray-transfer-matrix fashion, the formalism can be further expanded by introducing matrices similar to those proposed by Kostenbauder [19].

To address the beam steering we use a perturbative approach around the center wavelength λ_c for a known stable resonator mode Q_0. This is executed by altering the wavelength of this resonator mode to $\lambda = \lambda_c + \delta\lambda$ $(Q_0 \rightarrow \tilde{Q}_0)$, and propagating it through the resonator. After one roundtrip we obtain a shifted or altered spatial mode $\tilde{Q}_1 \neq Q_1 = Q_0$. This equation is equivalent to the stability condition for the resonator at λ_c. As stated before, the mode mismatch after a round-trip arises from the beam steering of dispersive or diffractive elements, which consequently alter the beam angle and waist impinging on the cavity optical elements. To find an equivalent associated loss (for relatively small steering) we calculate the overlap integral between $\tilde{Q}_1$ and $\tilde{Q}_0$. The efficiency parameter $\eta(\lambda)$ is equivalent to the first-order wavefunction coupling between the perturbed mode and the resonator mode. This coupling efficiency can be calculated as:

$$\eta(\lambda) = \frac{\left| \iint \Psi\left(\tilde{Q}_0(\lambda)\right) \bar{\Psi}\left(\tilde{Q}_1(\lambda)\right) \mathrm{d}A \right|^2}{\iint \left|\Psi\left(\tilde{Q}_0(\lambda)\right)\right|^2 \mathrm{d}A \cdot \iint \left|\Psi\left(\tilde{Q}_1(\lambda)\right)\right|^2 \mathrm{d}A}. \tag{4}$$

2.2. Transient gain response $\Gamma(t, \lambda)$

In this section we provide an overview of the gain dynamics in nanosecond pulsed laser systems operating in gain- or Q-switched mode. These lasers operate with optical gain well above the losses, either by intense pumping or by accumulating a large inversion of population ΔN in an otherwise low quality factor resonator [26]. The small-signal gain can be easily calculated using the emission- (σ_e) and absorption- (σ_a) cross-sections at the wavelength λ, and the population inversion ΔN as:

$$g(t, \lambda) = \Delta N(t) \cdot (\sigma_e(\lambda) - \sigma_a(\lambda)) - \Lambda_{NL}(t, \lambda). \tag{5}$$

Effects like excited state absorption (ESA) or upconversion usually introduce additional time-dependent losses $\Lambda_{NL}(t, \lambda)$, although this depends heavily on the choice of laser gain media. Under the assumption that $\Lambda_{NL}(t, \lambda)$ is only weakly dependent on wavelength, the net round-trip gain $\Gamma(t, \lambda)$ can be directly calculated taking into account $g(t, \lambda)$, the output coupler reflectivity R_{OC}, and general losses Λ as:

$$\Gamma(t, \lambda) = \mathrm{e}^{2\int_0^L g(t,\lambda)\mathrm{d}z} \cdot R_{OC} \cdot (1 - \Lambda(\lambda)). \tag{6}$$

where L denotes the length of the laser active medium. For a mode to build up in a laser the gain has to overcome the losses, resulting in the condition $\Gamma(\lambda) > 1$. This can be given for multiple modes, rising from vacuum fluctuations or thermal/electronic noise during the build-up phase of a laser pulse. Modes above lasing threshold will grow in intensity with their respective net gain, resulting in faster growth for modes with higher gain. Assuming homogeneous broadening, the mode competition and subsequent gain depletion are governed by the function $\Gamma(\lambda)$. For gain media with spectrally broad stimulated emission cross section, the gain function can further be assumed to be spectrally flat in the vicinity of the central wavelength λ_c. This way the mode competition close to λ_c is mainly influenced by $\Lambda(\lambda) = 1 - \Theta(\lambda)$.

In the following sections we provide a methodology to calculate $\alpha_{\mathbf{P}}(\lambda)$, $\eta(\lambda)$, and show an example of its application including gain dynamics.

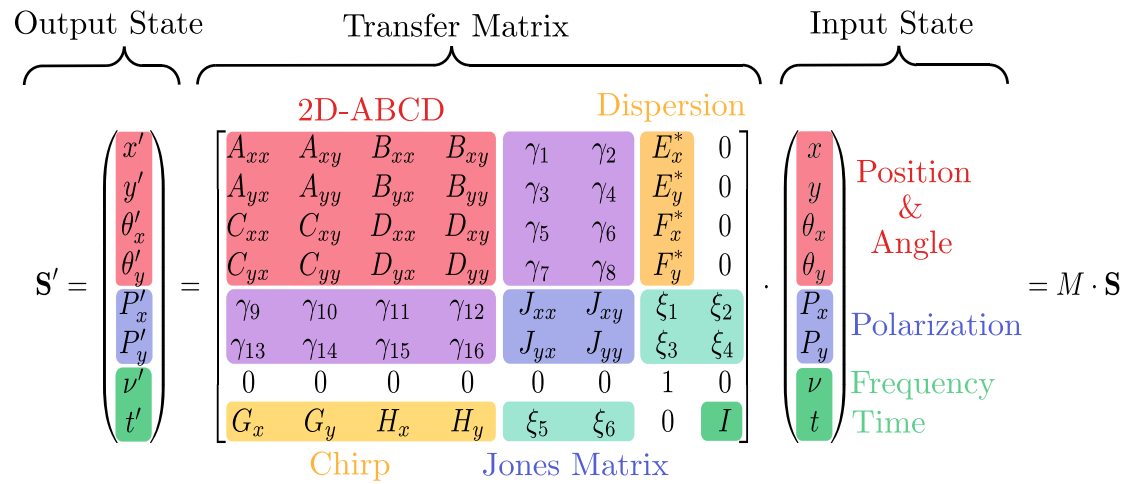

Figure 2. Composite ray transfer matrix formalism, showing the state of a ray in the input and output plane of an optical system. The state is a direct sum of the ray space **R**, containing transverse position and angle (red), polarization **P** (blue) and time and frequency (green). The transfer-matrix is similarly constructed as the direct sum of 2D-ABCD- and Jones-Matrix and the spatio-temporal extension of Kostenbauder [19]. Analogously to the dispersion and chirp terms (orange) included by Kostenbauder we introduce possible cross-talk terms between polarization and ray space γ_i, ξ_i and ϕ_i (purple and cyan).

3. Mathematical implementation

As mentioned, most of the existing tools used to describe optical systems are based on ray-transfer matrix formalisms. In this work, we extend these approaches into a unified formalism that incorporates beam propagation, polarization, and dispersion.

A description of such matrix and their relation to the components of the laser resonator is shown in figure 2. The matrix elements, apart from the newly introduced spatio-polarization interaction terms, can be found by applying the usual methods from 2D-ABCD (in red), Jones (in blue) and Kostenbauder (in orange and green) matrices [19]. This way we can describe many types of cavity elements, including mirrors, lenses, prisms, gratings, filters and polarization optics in one single model. Furthermore, the complex behavior like polarization dependent diffraction efficiencies of gratings can be included. We include possible interactions between polarization and ray position-angle γ_i (purple), and polarization and frequency–time ξ_i (cyan). The matrix elements γ_1 to γ_8 describe the change of the output ray position and angle as a function of input polarization. Even though there are optical elements capable of polarization dependent steering without beam splitting [28], γ_1 to γ_8 are zero for most common optical elements used in laser resonators. The elements γ_9 to γ_{16} could in principle describe anisotropic phase retardation arising from stress induced birefringence, leading to depolarization losses and a decrease in Strehl ratio below 1. In this scenario the transfer matrix formalism is limited to ray tracking, since it is not possible to calculate an associated complex beam parameter (q). The polarization-time coupling elements in the matrix (ξ_i) enable the modeling of polarization rotation as a function of time, such as when slow (compared to the cavity round-trip time) electro-optic modulators are employed. Due to the approach of a transfer matrix as linear theory, the description of the mentioned effects is limited to the linear contribution with respect to spatial and polarization coordinates. In our calculations we have neglected the spatio-polarization and polarization-time-frequency contributions in the components of our existing laser cavities described in section 4, as they do not induce any of the aforementioned optical effects.

Each single element in the laser resonator, as well as the space between them, is described by one of these transfer matrices *M*. Subsequent propagation through optical elements can be achieved by multiplying the transfer matrices in order of appearance. In this way the construction of more complex elements can be broken down into smaller pieces, and a composite RTM for the entire resonator can be found.

3.1. Power retention in an arbitrary polarization state

The Jones part of our RTM acts on the electric–field components of each axial mode, determining the polarization state and carrying information about the field amplitude. In our model, we also include any losses from optical components or material absorption in the Jones matrix *J*.

For an arbitrary (not necessarily normalized) polarization state **P**, the quantity of interest is the power that remains in the same polarization state after a round trip. This is obtained by projecting the output field $J_{\mathrm{RTM}}(\lambda)\mathbf{P}$ onto the direction of **P** and taking the modulus squared. The resulting round–trip power retention factor is:

$$\alpha_{\mathbf{P}}(\lambda) = \frac{\left|\mathbf{P}^{\dagger} J_{\mathrm{RTM}}(\lambda)\,\mathbf{P}\right|^{2}}{\left(\mathbf{P}^{\dagger}\mathbf{P}\right)^{2}}. \tag{7}$$

Here, the symbol † denotes the Hermitian (conjugate) transpose, i.e. complex conjugation followed by matrix transposition, as required for inner products between Jones vectors. The expression remains valid even when **P** is not an eigenvector of *J*, and provides a direct measure of the polarization-dependent feedback of the resonator. If no mode-steering elements are present, the analysis of $\alpha_{\mathbf{P}}$ is sufficient to determine the output polarization of the laser.

3.2. Resonator stability

For $\lambda = \lambda_c$ the stability criteria for a resonator mode can be checked and a stable Gaussian beam can be found from the 2D-ABCD part of the RTM [26]. In other words, to find a stable resonator configuration, we ensure that the roundtrip complex beam parameter Q_1 is identical to the input beam parameter Q_0 at λ_c.

The Kostenbauder formalism defines the dispersion terms (E and F) at each wavelength of the light, yielding a wavelength dependent spatial displacement. Here, we set $E_x^*(\lambda_c) = E_y^*(\lambda_c) = F_x^*(\lambda_c) = F_y^*(\lambda_c) \equiv 0$ to fulfil the resonance condition at the central wavelength λ_c. Therefore, we modify the dispersion terms (E and F in the Kostenbauder matrix) to represent only relative dispersion with respect to the central wavelength. We can define $E_x^*(\lambda) = E_x(\lambda) - E_x(\lambda_c)$ and similarly E_y^*, F_x^* and F_y^*, so that the resonance of a beam in the oscillator occur at the central wavelength.

This Gaussian beam, represented by the complex beam parameters $q_{x,y}$ will be used to describe the fundamental spatial mode of the resonator Q_0, following the notation of Alda *et al* [27]. With mode steering elements within the resonator a stable mode for $\lambda \neq \lambda_c$ cannot exist geometrically. However, that does not imply that the feedback provided by the resonator is 0, but rather would become a leaky or lossy resonator mode.

3.3. Implementation of the coupling losses

Now, to mathematically quantify the feedback contribution from mode steering, we consider the propagation of a TEM_{00} mode. According to Bayer-Helms [29], in a mismatched or misaligned system, the incident field does not coincide with the eigenmodes of the optical resonator. In this general situation, the incident wave can be expressed as a sum of eigenfunctions of a fictitious resonator whose configuration (mismatch) and orientation (misalignment) differ from those of the actual resonator.

Following this approach, each round trip is treated as an incoming beam with its own phase–space coordinates. For every pass, we evaluate the coupling between this incoming beam and the cavity's fundamental mode using the Bayer-Helms coupling parameters $k_{m,n}^{(x,y)}$. Figure 3 shows a schematic depiction of the influence of cavity mismatch after a round trip on the coupling loss. Mathematically, combining equation (7) and the mode coupling parameters for each axis, the total resonator feedback function can be written as:

$$\Theta_{\mathbf{P}}(\lambda) = \left|k_{0,0}^{(x)} k_{0,0}^{(y)}\right|^{2} \frac{\left|\mathbf{P}^{\dagger} J_{\mathrm{tot}}(\lambda)\,\mathbf{P}\right|^{2}}{\left(\mathbf{P}^{\dagger}\mathbf{P}\right)^{2}}. \tag{8}$$

3.4. Optical gain estimation

At the center lasing wavelength λ_c and a convenient polarization state **P**, the feedback function $\Theta(\lambda_c)$ has a local maximum. The width of that maximum will give a first upper limit for the laser linewidth as spectral modes far away from the maximum will be below lasing threshold. To get a more accurate estimate, the time resolved laser rate equations simulation has to be carried out. A model presented by M. Eichhorn can be slightly modified to account for multiple axial modes lasing independently [30]. The spectral sampling points j at λ_j described in [30] are chosen to coincide with the longitudinal modes of the resonator to get the power distribution among the respective modes, hence, the linewidth. On the high reflectivity mirror (HR) side of the resonator we apply $I_{s,j}^{+} = \Theta_{\mathbf{P}}(\lambda_j) \cdot I_{s,j}^{-}$ to account for the

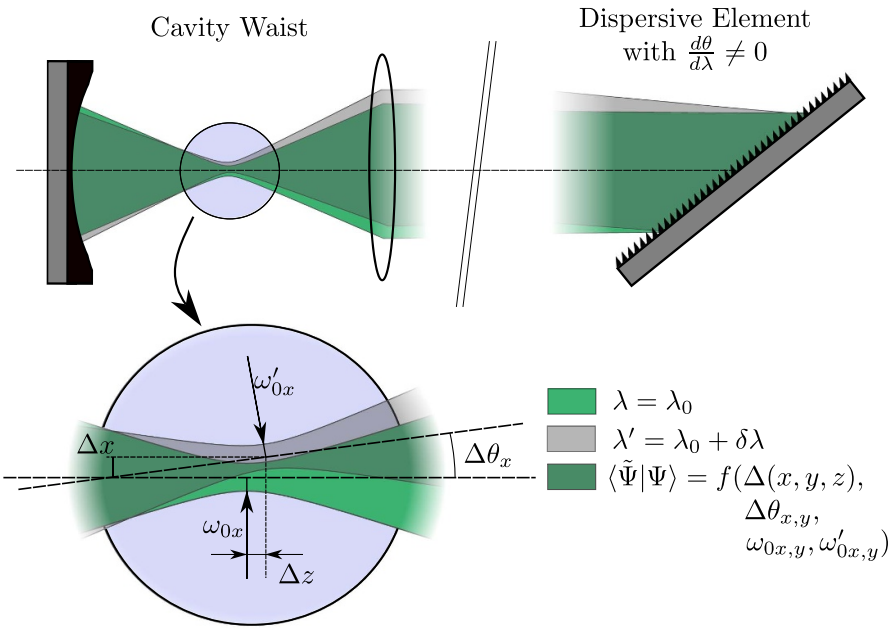

Figure 3. Schematic illustrating the feedback contribution from mode steering: a TEM_{00} incident beam, when mismatched or misaligned with the resonator due to a shift in wavelength, is decomposed into eigenmodes of a fictitious resonator. Each round trip is treated as an incoming beam with updated phase-space coordinates, and the overlap with the cavity's fundamental mode is evaluated using the Bayer–Helms formalism to compute the total resonator feedback in the spectral domain.

resonator feedback instead of solely using the HR mirror reflectivity. To keep computing times reasonable only longitudinal modes at wavelengths close to λ_c are used. Tests with a first crude implementation of a time resolved simulation show it is usually enough to include modes with a feedback of $\Theta > 0.9 \cdot \max(\Theta)$.

4. Benchmarking with experimental results

To evaluate the performance of the proposed model, we simulated several existing Ti:Sapphire laser configurations, each based on a z-folded resonator geometry with an optical cavity length of $L \approx 510\,\text{mm}$ and a folding angle of $\alpha_{\text{fold}} = 17.5°$. Two concave folding mirrors with a radius of curvature of $ROC = 75\,\text{mm}$ result in a mode diameter of $56\,\mu\text{m}$ in the crystal and two collimated regions with a diameter of $\approx 750\,\mu\text{m}$. The laser active medium is a Brewster-cut Titanium doped Sapphire crystal of $L_{\text{Crystal}} = 20\,\text{mm}$ length.

For the gain–loss simulation a doping concentration of $\approx 0.04\,\text{at\%}$ was assumed, an absorption cross-section of $\sigma_a(\lambda = 532\,\text{nm}) = 5 \cdot 10^{-20}\,\text{cm}^2$ and an emission cross-section $\sigma_e(\lambda)$ were taken from [31]. Further, ESA and residual ground state absorption around the laser wavelength $\sigma_a(\lambda \approx 775\,\text{nm})$ are considered to be negligible. The lasers are pumped from one side using a commercial ns Q-switched laser at 532 nm, producing 15 W of average power at 10 kHz repetition rate and 200 ns pulse duration. Optical coatings and dispersive element parameters were taken directly from datasheets. Material data such as refractive indices for all optics the beam passes through were calculated using their respective Sellmeier equations.

An overview of the modeled setups is shown in figure 4. Two different arrangements were considered: Littrow-Grating and Lyot Filter. In the Lyot Filter configuration, we considered two different setups (A and C), and are comprised of a BRF combined with etalons. In the Littrow-Grating a single setup (B) is considered. These setups resemble the main types of Ti:Sapphire lasers used in the ISOLDE facility at CERN and the RISIKO mass-seperator at JGU in Mainz, Germany. The input parameters for our simulation were taken from [11], and the simulation results were compared to the experimental results found in [1, 7, 11, 32, 33].

For setups A and C, the BRF consists of 3 quartz plates, with thicknesses of 0.3 mm, 1.2 mm and 4.8 mm. In test-setup A, a single glass etalon with a thickness of 0.3 mm and 40 % reflectivity n both sides is added to the BRF. The setup C extends the setup A by introducing a second uncoated etalon

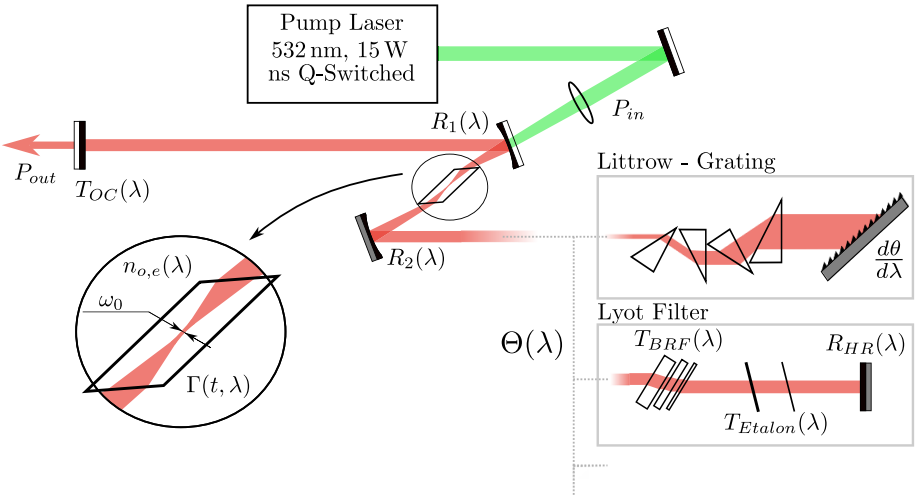

Figure 4. Schematic of the simulated Ti:Sapphire laser configurations. The general z-fold cavity layout interchangeable sections for implementation of spectral filtering schemes and wavelength dependent coatings and material properties. One scheme is employing a four-prism beam expander with a Littrow-mounted diffraction grating introducing angular dispersion. The other scheme is using a birefringent filter (BRF), one or two solid etalons, and a high-reflective end mirror.

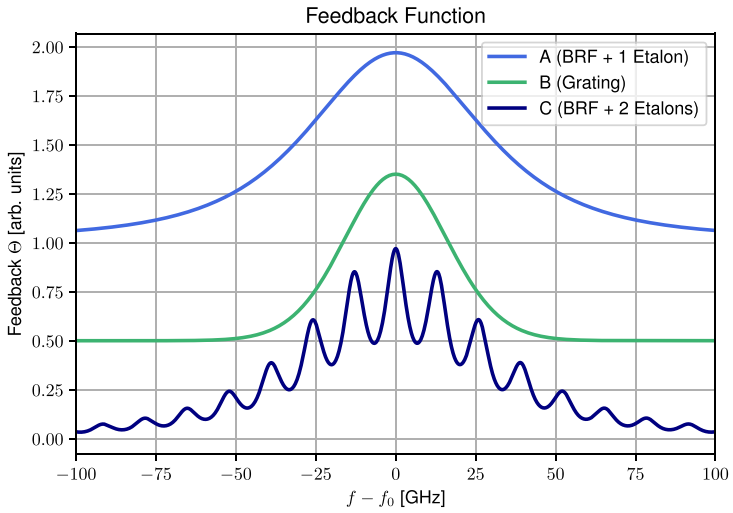

Figure 5. Feedback function of the described test setups around the central wavelength of 775 nm. The functions are vertically offset by 1, 0.5 and 0 for the setups A, B and C, respectively. For setup C with the 6.35 mm YAG etalon, the ∼ 13 GHz free spectral range of the etalon is visible as additional modulation.

made of YAG with thickness 6.35 mm. Setup B selects the wavelength with a ruled diffraction grating in Littrow configuration and a fourfold prism beam expander. The grating has a line density of 2000 lines/mm and a diffraction efficiency of ≈ 85 %.

For each test setup, the resonator feedback function $\Theta(\lambda)$ was computed at a central wavelength $\lambda_c = 775$ nm. The feedback functions around λ_c are shown in figure 5. The calculated feedback has been taken as input for a time and spatially resolved rate-equation modeling in the axial direction. Transverse dimensions have been neglected for simplicity in the simulation. The temporal profile of the pump pulse has been taken from experimental data, while the intensities have been scaled to the incident pulse energy and focal spot size in the laser crystal. The simulation has been performed similarly to the method described by Eichhorn *et al* [30].

Figure 6 presents the model results regarding the spectral shape for each case. Table 1 summarizes the main results, including the linewidths extracted from the initial feedback function $\Theta(f)$, the narrowed function $\Theta^{\frac{\tau_c}{t_{rt}}}(f)$, the linewidth calculated from the simulation and from the experimentally measured laser spectrum for each configuration. The ratio of cavity lifetime τ_c and the cavity roundtrip time t_{rt} has been used to showcase the narrowing effect of the multiple passes through the cavity, as a photon

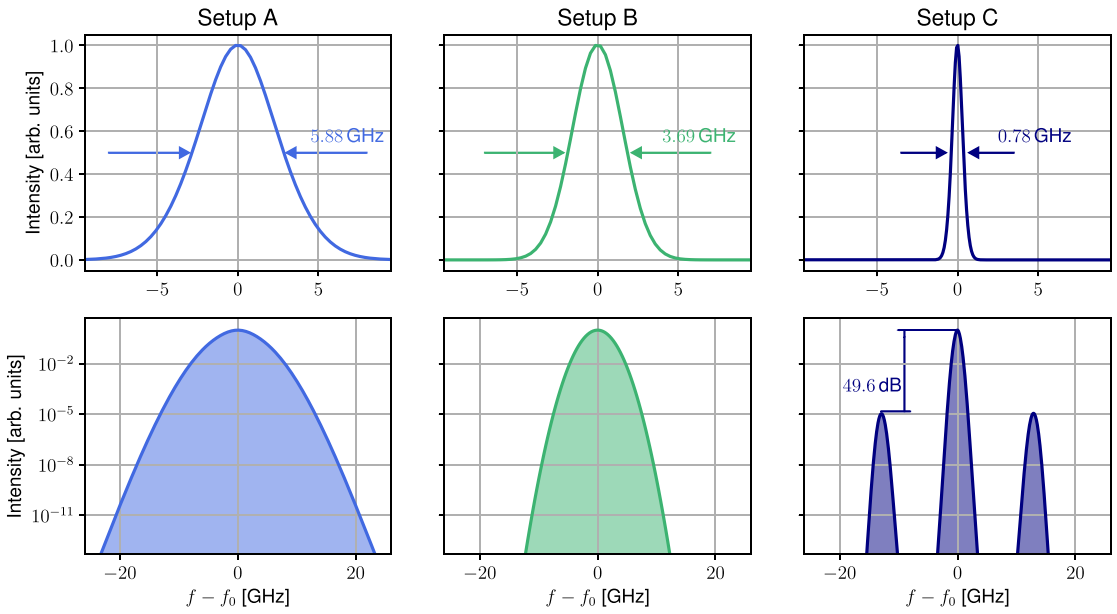

Figure 6. Simulated spectra of the three Ti:Sapphire laser configurations described in section 4. Setup A combines a three-plate quartz BRF (0.3/1.2/4.8 mm) with a 0.3 mm glass etalon (40% R), yielding a linewidth of 5.88 GHz. Setup B uses a Littrow grating (2000 lines/mm) with a 4× prism expander, giving 3.42 GHz. Setup C adds a 6.35 mm YAG etalon to Setup A, achieving a linewidth of 0.78 GHz and a side-mode suppression of 49.6 dB.

Table 1. FWHM linewidths of $\Theta(f)$, $\Theta^{\frac{\tau_c}{\tau_{rt}}}(f)$ and spectral intensity distribution after time resolved simulation for the different setups. The time resolved energetic simulations have been carried out with different pump fluences, ranging from half to double the experimentally present fluence. The displayed values are the mean and standard deviation of the obtained linewidths.

Setup	FWHM $\Theta(f)$ [GHz]	FWHM $\Theta(f)^{\frac{\tau_c}{\tau_{rt}}}$ [GHz]	simulated Δf [GHz]	measured Δf[GHz]
A	63.8	27.6	5.48 ± 0.51	5 [1, 32, 33], 5.6 [7], 4-8 [11]
B	38	17.9	3.42 ± 0.48	3.6 [7], 1-5 [32]
C	12.1	3.8	0.78 ± 0.07	0.8 [1], 1, 0.9, 0.6 [11]

will on average see this many filtering passes through Θ. The measured values are taken from previously published work [1, 7, 11, 32, 33].

5. Discussion and conclusion

We have presented a modeling approach for widely tunable narrow-linewidth laser resonator design that addresses key limitations in existing models. The technique is particularly valuable for constructing laser systems with linewidths in the MHz and GHz ranges. The model is rooted in the combination of well-known methods of ray propagation and mode-coupling in resonators. Together they are able to describe precisely the effect of intra-cavity dispersion and diffraction, and get realistic estimates for the resulting laser linewidth and optical power. Moreover, the agreement of simulation and experimental values for all setups showcases the capability of our model to estimate laser linewidth accurately. Its simplicity enables us to compare and optimize resonator designs with respect to achievable linewidth efficiently.

Even though this formalism provides a useful tool in understanding the effects of dispersion inside a laser resonator for gain switched lasers, its expansion towards ultrafast resonators is not trivial. The Kostenbauder / ABCD formalism, while often used to describe assemblies for ultrafast pulse compressors lacks of a precise wavelength resolved optical path length, necessary to calculate the true phase (or wavefront) of each spectral mode as well as non-linear effects. Likewise, sub-cavities and complex multi-cavity arrangements are beyond the scope of this model.

Further, some dispersive effects are not described in their full extent. For example the chromatic aberration of lenses in the cavity will change the original mode Q_0 depending on the wavelength [34].

This however, violates the assumption that Q_0 is unchanged from $\lambda = \lambda_c$ to $\lambda = \lambda_c + \delta\lambda$ for the calculation of the mode coupling losses. In the realm of a linear theory this can probably assumed to be a small perturbation and will not harm the overall validity of the model. Similar limitations will be present for spatial gain mode pulling effects inside the active medium.

An extension of the presented formalism to include transverse multi-mode behavior of lasers seems to be feasible. The coupling theory by Bayer-Helms supports coupling into higher order modes and the propagation of those modes using ray transfer matrices has also been demonstrated [35]. However, finding the stability condition of higher order modes with their respective center frequencies is necessary.

Future work involves the investigation of several potential extensions of the model. For example, including γ_i and ξ_i in M could enable the inclusion of interactions and effects where space and polarization are coupled. Optical elements like spatially varying waveplates and phase-plates, or thermally induced birefringence in crystals could be included at the cost of losing the ability to propagate Gaussian beams with the complex q-parameter, and so only pure ray tracing will be possible.

In terms of net gain–loss calculations, an upgrade of the rate-equation modeling is necessary to account for effects typically occurring in the DUV spectral range. These include ESA, color centers and two photon absorption. This will be crucial to get a more precise estimate for the linewidth achievable utilizing our Ce^{3+}:LiCAF laser, which aims to produce high-power tunable narrow-line in this hard to access spectral region.

Data availability statement

Data underlying the results presented in this paper can be obtained from the authors upon reasonable request. There is no experimental data produced in this study. Results and findings, as well as the working principle of the used simulation are reported within this paper and the supplementary material. The data that support the findings of this study are available upon reasonable request from the authors.

Examples and Results available at https://doi.org/10.1088/2515-7647/ae6496/data1.

Conflicts of interest

The authors declare no conflicts of interest.

Author contributions

Hendrik Büker 0009-0005-7959-9224
Conceptualization (equal), Data curation (equal), Formal analysis (equal), Investigation (equal), Methodology (equal), Validation (equal), Visualization (equal), Writing – original draft (equal), Writing – review & editing (equal)

Marc Eichhorn
Funding acquisition (equal), Investigation (equal), Methodology (equal), Project administration (equal), Resources (equal), Supervision (equal), Validation (equal)

Katerina Chrysalidis 0000-0003-2908-8424
Funding acquisition (equal), Project administration (equal), Resources (equal), Supervision (equal), Validation (equal), Writing – review & editing (equal)

Eduardo Granados 0000-0002-6549-9303
Conceptualization (equal), Formal analysis (equal), Investigation (equal), Methodology (equal), Project administration (equal), Resources (equal), Validation (equal), Writing – original draft (equal), Writing – review & editing (equal)

References

[1] Fedosseev V, Chrysalidis K, Goodacre T D, Marsh B, Rothe S, Seiffert C and Wendt K 2017 *J. Phys. G: Nucl. Part. Phys.* **44** 084006
[2] Heinke R *et al* 2023 *Nucl. Instrum. Methods Phys. Res. B* **541** 8–12
[3] Granados E, Stoikos G, Bernerd C, Chrysalidis K, Echarri D T, Fedosseev V N, Heinke R and Marsh B A 2024 *Laser Photonics Rev.* **18** 2300564
[4] Sonnenschein V, Moore I D, Raeder S, Reponen M, Tomita H and Wendt K 2017 *Laser Phys.* **27** 085701

[5] Granados E, Granados C, Ahmed R, Chrysalidis K, Fedosseev V N, Marsh B A, Wilkins S G, Mildren R P and Spence D J 2022 *Optica* **9** 317
[6] Chrysalidis K *et al* 2020 *Nucl. Instrum. Methods Phys. Res. B* **463** 476–81
[7] Echarri D T, Chrysalidis K, Fedosseev V N, Heinke R, Marsh B A, Reich B B and Granados E 2022 *Front. Phys.* **10** 937976
[8] Chrysalidis K, Fedosseev V N, Marsh B A, Mildren R P, Spence D J, Wendt K D A, Wilkins S G and Granados E 2019 *Opt. Lett.* **44** 3924
[9] Echarri D T, Chrysalidis K, Fedosseev V N, Marsh B A, Mildren R P, Olaizola S M, Spence D J, Wilkins S G and Granados E 2020 *Opt. Express* **28** 8589
[10] Coutts D and McGonigle A 2004 *IEEE J. Quantum Electron.* **40** 1430–40
[11] Rothe S 2013 *An all-Solid State Laser System for the Laser ion Source Rilis and in-Source Laser Spectroscopy of Astatine at Isolde* (CERN)
[12] Duarte F J 1992 *Opt. Quantum Electron.* **24** 49–53
[13] Collins S A 1970 *J. Opt. Soc. Am.* **60** 1168
[14] Kogelnik H 1965 *Bell Syst. Tech. J.* **44** 455–94
[15] Duarte F and Piper J 1982 *Opt. Commun.* **43** 303–7
[16] Duarte F J and Piper J A 1983 *Am. J. Phys.* **51** 1132–4
[17] Duarte F J and Piper J A 1984 *Appl. Opt.* **23** 1391
[18] Martinez O 1989 *IEEE J. Quantum Electron.* **25** 296–300
[19] Kostenbauder A 1990 *IEEE J. Quantum Electron.* **26** 1148–57
[20] Martínez O E and Chilla J L A 1992 *Opt. Lett.* **17** 1210
[21] Marcus G 2016 *Opt. Express* **24** 7752
[22] Worku N G and Gross H 2020 *J. Opt. Soc. Am. A* **37** 797
[23] Zhu X and Diels J C 2024 *Appl. Opt.* **63** 904
[24] Büker H, Granados E, Chrysalidis K and Eichhorn M 2025 *Method to Calculate Resonator Losses Including Diffractive Elements Optica Laser Congress Congress 2025* (Optica Publishing Group) p JW2A.42
[25] Saleh B E A and Teich M C 1991 *Polarization and Crystal Optics Fundamentals of Photonics* (Wiley) pp 193–237
[26] Siegman A 1986 *Lasers* 1st edn (University Science Books)
[27] Alda J, Wang S and Bernabeu E 1991 *Opt. Commun.* **80** 350–2
[28] Hoy C, Stockley J, Shane J, Kluttz K, McKnight D and Serati S 2021 *Crystals* **11** 361
[29] Bayer-Helms F 1984 *Appl. Opt.* **23** 1369–80
[30] Eichhorn M 2008 *IEEE J. Quantum Electron.* **44** 803–10
[31] Sorokin E and Kärtner F X 2004 *Solid-State Materials for few-Cycle Pulse Generation and Amplification Few-Cycle Laser Pulse Generation and its Applications* (Springer) pp 3–73
[32] Studer D, Dyrauf P, Naubereit P, Heinke R and Wendt K 2017 *Hyperfine Interact.* **238** 8
[33] Fedosseev V N *et al* 2012 *Rev. Sci. Instrum.* **83** 02A903
[34] Martí-López L and Mendoza-Yero O 2001 *Opt. Laser Technol.* **33** 1–5
[35] Lü B, Zhang B and Cai B 1993 *J. Mod. Opt.* **40** 1731–43